A weighted variational model for simultaneous reflectance and illumination estimation

Xueyang Fu[1,2], Delu Zeng[1,2], Yue Huang[1,2], Xiao-Ping Zhang[1,3], Xinghao Ding[1,2*]

[1]Fujian Key Laboratory of Sensing and Computing for Smart City, Xiamen University, China

[2]School of Information Science and Engineering, Xiamen University, China

[3]Department of Electrical and Computer Engineering, Ryerson University, Canada

fxy@stu.xmu.edu.cn, {dltsang, yhuang2010}@xmu.edu.cn, xzhang@ee.ryerson.ca, dxh@xmu.edu.cn

Abstract

We propose a weighted variational model to estimate both the reflectance and the illumination from an observed image. We show that, though it is widely adopted for ease of modeling, the log-transformed image for this task is not ideal. Based on the previous investigation of the logarithmic transformation, a new weighted variational model is proposed for better prior representation, which is imposed in the regularization terms. Different from conventional variational models, the proposed model can preserve the estimated reflectance with more details. Moreover, the proposed model can suppress noise to some extent. An alternating minimization scheme is adopted to solve the proposed model. Experimental results demonstrate the effectiveness of the proposed model with its algorithm. Compared with other variational methods, the proposed method yields comparable or better results on both subjective and objective assessments.

1. Introduction

Observed images can be decomposed as a product of reflectance and illumination using a simplified physical model of light reflection [14]. In such a decomposition, the illumination represents the light intensity on the objects in the image, and the reflectance represents the physical characteristics of objects. There are many applications derived from this decomposition, such as ordinary image enhancement [24, 33, 3, 9], high dynamic range image tone mapping [7, 29], remote sensing image correction [12] and target selection and tracking [18, 10].

Since estimating the reflectance and the illumination from a single observed image is an ill-posed inverse problem [14], a number of modeling approaches have been developed to incorporate prior structural assumptions. For example, [14, 13] propose path-based algorithms. These methods require intensive parameter tuning and have high computational complexity, which was later addressed using recursive matrix calculation [5, 21]. Another family of methods use partial differential equations (PDE) [8, 23], which can be solved efficiently using the fast Fourier transformation (FFT). In [38], a nonlocal texture constraint is adopted for decomposing intrinsic images.

Recently, several variational methods have been presented. In [11], Kimmel et al. propose a variational model to estimate the illumination, which is assumed varies smoothly. The assumption of the reflectance is not considered in the model. In [20], a total variation (TV) and nonlocal TV regularized model, solved by adopting Bregman iteration, is developed and studied. An L1-based variational model is further introduced in [19] to focus on estimating the reflectance. In [26], a TV model for image decomposition by considering both reflectance and illumination components in the objective function is proposed. The model is divided into two sub-problems and solved by the split Bregman method. However, this method may result in an over-smoothed reflectance due to the side effect of the logarithmic transformation. This method is complemented by using nonlocal bounded variation [35] to achieve an effective decomposition of illumination and reflectance. Following [26], a variational model with barriers for image decomposition is proposed in [34]. The model is defined as a constrained optimization problem associated with the deduced energy functional. In [16], an adaptive perceptually inspired variational model is developed to recover the reflectance and to adjust the uneven intensity distribution. However, the computational cost of this method is high; processing a 1000×1000 image requires about 10 minutes. A kernel-based variational model is introduced in [2]. An analysis of this model on contrast is provided in the literature. This method can deal with color cast and enhance both under- and over-exposed images. A perception based

*Correspondence author.

color correction of digital images in the variational framework is presented in [28, 1]. Both color enhancement and local contrast improvement can be achieved in this method. Meanwhile, a numerical implementation of the gradient descent technique is also shown in these works. Another approach based on a variational Bayesian method is proposed in [32]. In this literature, the variational Bayes approximation approach is adopted to estimate both the illumination and the reflectance. However, finer details of the estimated reflectance are lost due to the logarithmic transformation. In addition, the computational cost is high since it requires calculations of some linear equations. In [17], a higher order TV model for estimating the reflectance and the illumination is proposed. The primal-dual splitting algorithm, which needs to many iterations, is adopted to solve the model. Based on nonlocal differential operators, a unifying model focuses on the reflectance is proposed in [39].

Most of the above variational methods use the logarithmic transformation for pre-processing not only to reduce the computational complexity [30] but also to simulate human vision perception mechanism, such as Weber's law [31]. Using the logarithmic transformation to model the fidelity term is proper since the process simulates human eye perception of light intensity. However, since the logarithmic transformation suppresses the variation of gradient magnitude in bright regions, using the gradient in logarithmic domain as the regularization terms is not proper. In other words, solving the ill-posed problem by adopting these regularization terms may lead to an undesirable result, such as loss of finer details in the estimated reflectance.

In this paper, a weighted variational model for simultaneously estimating reflectance and illumination is presented. First, by analyzing the characteristic of the logarithmic transformation, we show that the logarithmic transformation is not proper to be directly used as regularization terms. Then, based on the previous analysis, a weighted variational model is introduced for better prior representation and an alternating minimization scheme is adopted to solve the proposed model. Unlike existing variational methods using complex techniques, such as nonlocal techniques [35] and dictionary learning techniques [3], the proposed model can achieve significant improvement by simply weighting the widely used regularization terms. Compared with classical variational models, the proposed model can preserve the estimated reflectance with more details. Moreover, the proposed model can suppress noise to some extent. An alternating minimization scheme is adopted to solve the proposed model. Experimental results demonstrate the effectiveness of the proposed model with its algorithm. Compared with other variational methods, the proposed method yields comparable or better results on both subjective and objective assessments.

2. Background: Discussion on log-transform

The physical model of light reflection can be simply described as $\mathbf{S} = \mathbf{R} \cdot \mathbf{L}$, where $\mathbf{S}$ is the observed image, $\mathbf{R}$ is the reflectance of the image within the range $(0, 1]$, and $\mathbf{L}$ is the illumination within the range $(0, \infty)$. The dot "$\cdot$" denotes pixel-wise multiplication and all images are vectorized. It follows that $\mathbf{S} \leq \mathbf{L}$. The goal is to estimate the reflectance $\mathbf{R}$ and the illumination $\mathbf{L}$ from the observed image $\mathbf{S}$.

To this end, most variational methods first transform $\mathbf{S} = \mathbf{R} \cdot \mathbf{L}$ into the logarithmic domain, $\mathbf{s} = \mathbf{r} + \mathbf{l}$, where $\mathbf{s} = \log(\mathbf{S})$, $\mathbf{r} = \log(\mathbf{R})$ and $\mathbf{l} = \log(\mathbf{L})$. Using this logarithmic transformation, the first variational algorithm for this decomposition was proposed in [11]. This approach only models the illumination $\mathbf{l}$ and then estimates the reflectance $\mathbf{R}$ by $\exp(\mathbf{s} - \mathbf{l})$ in post-processing. Another variational method [26] considers both illumination and reflectance in the objective function, which is arguably more appropriate. However, the directly estimated reflectance images are typically too smooth and loose much of the desired edges and texture details. In [26], the authors abandon the directly estimated reflectance and instead use $\exp(\mathbf{s} - \mathbf{l})$.

Our goal is to develop an objective function that outputs a usable illumination and reflectance. To this end, we observe that conventional methods use an objective function along the following lines:

$$E(\mathbf{r}, \mathbf{l}) = \|\mathbf{l} + \mathbf{r} - \mathbf{s}\|_2^2 + \lambda_1 \|\nabla \mathbf{l}\|_2^2 + \lambda_2 \|\nabla \mathbf{r}\|_1 \quad s.t.\ \ \mathbf{r} \leq 0 \ \text{ and } \ \mathbf{s} \leq \mathbf{l}. \tag{1}$$

In this objective function, the logarithmic illumination $\mathbf{l}$ uses a squared penalty to enforce spatial smoothness and the logarithmic reflectance $\mathbf{r}$ is encouraged to be piece-wise constant using L1-norm. The fidelity term is the squared error term between the log-transformed image and its breakdown in illumination and reflectance.

Since the logarithmic transform conforms with human perception of light intensity as described by Weber's law [31], it is appropriate to use the logarithmic transformed image to define the fidelity term. However, we argue that the logarithmic transform is not appropriate in the penalty terms on $\mathbf{l}$ and $\mathbf{r}$, since it magnifies errors in certain ranges more than others. More specifically, given a target stimulus signal x, its gradient variation is ∇x, and, while in the log-transformed domain it is $\nabla(\log(x)) = \frac{1}{x}\nabla x$. Therefore, when x is very small, the gradient variation in the log-transform $\nabla(\log(x))$ is highly weighted by $\frac{1}{x}$. While this too agrees with Weber's law, when the variation $\nabla(\log(x)) = \frac{1}{x}\nabla x$ is used in a norm penalty, it inevitably dominates over the variation term in the high magnitude areas. This is not desirable when we estimate/recover the fine details in the high magnitude stimuli areas as well.

Such phenomenon is illustrated in Fig 1. As shown in Fig. 1(b), much structure is amplified in low magnitude s-

(a) input and log-transformed (b) corresponding gradients of (a)

Figure 1. Example of logarithmic transformation.

timuli areas in the log-transformed domain, indicating that these areas are highly weighted by $\frac{1}{x}$. We can see that, when minimizing a norm over this entire image, the intensity of fine edges and details in high illumination areas will be buried in irrelevant details in low illumination areas. This scaling of intensities will make estimating/recovering fine structures in these areas more challenging.

To preserve edges and details, most existing variational methods use the estimated illumination to estimate the reflectance using the equation $\mathbf{R} = \mathbf{S}/\mathbf{L}$ in post-processing. However, any error in estimated illumination at a pixel, will clearly affect the estimated reflectance at the same location. Intuitively, we argue that a method which can estimate illumination and reflectance simultaneously and accurately should be considered. Based on the above discussion, we also argue that the gradient variation in the log-transformed domain is not proper as a regularization term. In the next section we present a weighted variational model to address this, and derive an alternating minimization algorithm to estimate the illumination and reflectance simultaneously.

3. Model and Algorithm

As described above, a loss of fine details is incurred by the weight $\frac{1}{x}$ in $\nabla(\log(x)) = \frac{1}{x}\nabla x$ when penalizing the log-transform domain. For better prior representation, it is natural to modify the form of $\nabla(\log(x))$, i.e., the regularization terms, to eliminate the weight's impact. Based on the widely used assumptions, a new objective function is established by weighting the regularization terms:

$$E(\mathbf{r},\mathbf{l}) = \|\mathbf{r}+\mathbf{l}-\mathbf{s}\|_2^2 + c_1\|e^{\mathbf{r}}\cdot\nabla\mathbf{r}\|_1 + c_2\left\|e^{\mathbf{l}}\cdot\nabla\mathbf{l}\right\|_2^2 \quad s.t.\ \mathbf{r}\le 0 \text{ and } \mathbf{s}\le\mathbf{l}, \tag{2}$$

where c_1 and c_2 are positive parameters, $\|\|_p$ denotes the p-norm operator. To minimize E($\mathbf{r}$, $\mathbf{l}$), for the first term ($\|\mathbf{r}+\mathbf{l}-\mathbf{s}\|_2^2$), which corresponds to L2 data fidelity, is to minimize the distance between estimated $(\mathbf{r}+\mathbf{l})$ and observed image $\mathbf{s}$. The second term ($\|e^{\mathbf{r}}\cdot\nabla\mathbf{r}\|_1$), which corresponds to TV reflectance sparsity, enforces piece-wise constant on the reflectance $\mathbf{r}$. The third term ($\left\|e^{\mathbf{l}}\cdot\nabla\mathbf{l}\right\|_2$) enforces spatial smoothness on the illumination $\mathbf{l}$. Note that the $\nabla\mathbf{r}$ and $\nabla\mathbf{l}$ are respectively weighted by $e^{\mathbf{r}}$ and $e^{\mathbf{l}}$ to eliminate the impact of $\frac{1}{\mathbf{R}}$ and $\frac{1}{\mathbf{L}}$.

Since $e^{\mathbf{r}}$ and $\nabla\mathbf{r}$ are coupled in the second term and $e^{\mathbf{l}}$ and $\nabla\mathbf{l}$ are coupled in the third term, minimizing the objective function (2) is difficult. However, eliminating the impact of the weights, i.e., $\frac{1}{\mathbf{r}}$ and $\frac{1}{\mathbf{l}}$, in regularization terms can better represent the prior knowledge. Thus, we build a new objective function which is easy to minimize, besides, it can effectively eliminate the impact of the weights. Note that $e^{\mathbf{r}} = \mathbf{R}$ and $e^{\mathbf{l}} = \mathbf{L}$ can be computed by using the previous results and seen as constant vectors. Based on this strategy, the new objective function at the kth iteration is:

$$E(\mathbf{r}^k,\mathbf{l}^k) = \left\|\mathbf{r}^k+\mathbf{l}^k-\mathbf{s}\right\|_2^2 + c_1\left\|\mathbf{R}^{k-1}\cdot\nabla\mathbf{r}^k\right\|_1 + c_2\left\|\mathbf{L}^{k-1}\cdot\nabla\mathbf{l}^k\right\|_2^2 \quad s.t.\ \mathbf{r}^k\le 0 \text{ and } \mathbf{s}\le\mathbf{l}^k, \tag{3}$$

Since there are two unknowns in the objective function, traditional gradient descent methods are unusable. In this paper, an alternating direction method of multipliers (ADMM) [6] is adopted to solve the objective function. For the L1-norm, an auxiliary variable $\mathbf{d}$ and an error $\mathbf{b}$ are introduced and function (3) is rewritten as:

$$E(\mathbf{r}^k,\mathbf{l}^k,\mathbf{d}^k,\mathbf{b}^k) = \left\|\mathbf{r}^k+\mathbf{l}^k-\mathbf{s}\right\|_2^2 + c_2\left\|\mathbf{L}^{k-1}\cdot\nabla\mathbf{l}^k\right\|_2^2 + c_1\{\left\|\mathbf{d}^k\right\|_1 + \lambda\left\|\mathbf{R}^{k-1}\cdot\nabla\mathbf{r}^k-\mathbf{d}^k+\mathbf{b}^k\right\|_2^2\} \quad s.t.\ \mathbf{r}^k\le 0 \text{ and } \mathbf{s}\le\mathbf{l}^k. \tag{4}$$

This objective function will have local minima according to ADMM theory [6]. Three separate sub-problems are iteratively cycled through. In particular, for the kth iteration:

$$(P1)\quad \mathbf{d}^k = \arg\min_{\mathbf{d}} \|\mathbf{d}\|_1 + \lambda\left\|\mathbf{R}^{k-1}\cdot\nabla\mathbf{r}^{k-1}-\mathbf{d}+\mathbf{b}^{k-1}\right\|_2^2,$$

$$(P2)\quad \mathbf{r}^k = \arg\min_{\mathbf{r}} \left\|\mathbf{r}+\mathbf{l}^{k-1}-\mathbf{s}\right\|_2^2 + c_1\lambda\left\|\mathbf{R}^{k-1}\cdot\nabla\mathbf{r}-\mathbf{d}^k+\mathbf{b}^{k-1}\right\|_2^2,$$
$$\mathbf{b}^k = \mathbf{b}^{k-1}+\mathbf{R}^k\cdot\nabla\mathbf{r}^k-\mathbf{d}^k,$$

$$(P3)\quad \mathbf{l}^k = \arg\min_{\mathbf{l}} \left\|\mathbf{l}+\mathbf{r}^k-\mathbf{s}\right\|_2^2 + c_2\left\|\mathbf{L}^{k-1}\cdot\nabla\mathbf{l}\right\|_2^2.$$

The three sub-problems have closed form global optimal solutions. The update for $\mathbf{b}^k$ follows from ADMM. The algorithm is detailed as follows:

1) Algorithm for $P1$ A shrinkage operation is adopted to update $\mathbf{d}^k$ at the kth iteration:

$$\mathbf{d}_h^k = shrink(\mathbf{R}^{k-1}\cdot\nabla_h\mathbf{r}^{k-1}+\mathbf{b}_h^{k-1}, \tfrac{1}{2\lambda}),$$
$$\mathbf{d}_v^k = shrink(\mathbf{R}^{k-1}\cdot\nabla_v\mathbf{r}^{k-1}+\mathbf{b}_v^{k-1}, \tfrac{1}{2\lambda}), \tag{5}$$

where $shrink(x,\lambda) = \frac{x}{|x|} * \max(|x| - \lambda, 0)$ with $\frac{x}{|x|}$ equal to 0 when $|x| = 0$. h and v are the horizontal and vertical directions, respectively.

2) Algorithm for $P2$ Since $P2$ is a least squares problem, $\mathbf{r}^k$ has a closed form solution. The Fast Fourier Transformation (FFT) is adopted to speed up the process. By setting the first-order derivative to zero, $\mathbf{r}^k$ is updated by the following expression:

$$\mathbf{r}^k = F^{-1}\left(\frac{F(\mathbf{s} - \mathbf{l}^{k-1}) + c_1\lambda\mathbf{\Phi}}{F(\mathbf{U}) + c_1\lambda\mathbf{R}^{k-1} \cdot (F^*(\nabla_h) \cdot F(\nabla_h) + F^*(\nabla_v) \cdot F(\nabla_v))}\right), \tag{6}$$

where $\mathbf{U}$ is the identity matrix, $\mathbf{\Phi} = F^*(\nabla_h) \cdot F(\mathbf{d}_h^k - \mathbf{b}_h^{k-1}) + F^*(\nabla_v) \cdot F(\mathbf{d}_v^k - \mathbf{b}_v^{k-1})$, F is the FFT operator, F^* is the conjugate transpose and F^{-1} is the inverse FFT operator. The derivative operator is diagonalized after FFT so that matrix inversion can be avoided. All calculations are performed pixel-wise. According to the prior: $\mathbf{r} \leq 0$, a simple correction is made after $\mathbf{r}^k$ is updated: $\mathbf{r}^k = \min(\mathbf{r}^k, 0)$.

Updating $\mathbf{b}^k$ by the following expression:

$$\begin{aligned} \mathbf{b}_h^k &= \mathbf{b}_h^{k-1} + \mathbf{R}^k \cdot \nabla_h \mathbf{r}^k - \mathbf{d}_h^k, \\ \mathbf{b}_v^k &= \mathbf{b}_v^{k-1} + \mathbf{R}^k \cdot \nabla_v \mathbf{r}^k - \mathbf{d}_v^k. \end{aligned} \tag{7}$$

This operation is the similar to "adding back the noise" used in TV denoising [27]. $\mathbf{d}$, $\mathbf{r}$ and $\mathbf{b}$ are updated until $\varepsilon_{\mathbf{r}} = \left(\left\|\mathbf{r}^k - \mathbf{r}^{k-1}\right\| / \left\|\mathbf{r}^{k-1}\right\|\right) \leq \varepsilon_1$.

3) Algorithm for $P3$ Since $P3$ is also a least squares problem, updating $\mathbf{l}^k$ is similar to $\mathbf{r}^k$:

$$\mathbf{l}^k = F^{-1}\left(\frac{F(\mathbf{s} - \mathbf{r}^k)}{F(\mathbf{U}) + c_2\mathbf{L}^{k-1}(F^*(\nabla_h) \cdot F(\nabla_h) + F^*(\nabla_v) \cdot F(\nabla_v))}\right). \tag{8}$$

According to the prior: $\mathbf{s} \leq \mathbf{l}$, a simple correction is made after $\mathbf{l}^k$ is updated: $\mathbf{l}^k = \max(\mathbf{l}^k, \mathbf{s})$. $\mathbf{l}$ is updated until $\varepsilon_{\mathbf{l}} = \left(\left\|\mathbf{l}^k - \mathbf{l}^{k-1}\right\| / \left\|\mathbf{l}^{k-1}\right\|\right) \leq \varepsilon_2$.

Since large-matrix inversion is avoided by FFT and the shrinkage operation is fast due to requiring only a few operations, $\mathbf{r}$ and $\mathbf{l}$ can be solved simultaneously and efficiently. The final estimated reflectance and illumination are obtained by $\mathbf{R} = e^{\mathbf{r}}$ and $\mathbf{L} = e^{\mathbf{l}}$, respectively. In the next section, experimental results are presented to demonstrate the effectiveness of the proposed method.

4. Experimental Results

All experiments are performed using our unoptimized Matlab implementation[1] on a PC with Intel Core i5 CPU 4460, 8GB RAM. We compare the proposed model with other two classical models: Kimmel's model [11] and Ng's model [26]. For fair comparison, the parameters used in the two methods are set to be optimal according to [11] and [26]. In our experiments, the empirical parameters c_1, c_2 and λ are set at 0.01, 0.1 and 1, respectively. For the stopping parameters, ε_1 and ε_2 are set to be 10^{-3}. The initial value $\mathbf{R}^0 = 0$, $\mathbf{b}^0 = 0$, $\varepsilon_{\mathbf{r}} = 10$ and $\varepsilon_{\mathbf{l}} = 10$. In general, there are two approaches for dealing with the color images [11, 26]. More precisely, one approach processes each color channel (Red, Green, and Blue) separately to improve the colors or correct color distortion. Another approach is to transform color images into the HSV (Hue, Saturation and Value) space and only process the V-channel, and then transform it back to the RGB domain.

Reflectance and Illumination Estimation First, two comparisons of reflectance and illumination estimation are shown in Figs. 2 and 3. Fig. 2 shows the comparison in the RGB domain and Fig. 3 shows the comparison in the HSV domain. Since the reflectance is not considered in Kimmel's model [11], only Ng's estimated reflectance [26] is shown. The results in Fig. 2 include color information since the algorithms are applied to each RGB channel separately. As can be seen, the illumination estimated by our model is more smooth than other two methods. In other words, our results are more conform with the illumination's prior of spatial smoothness. Though Ng's method [26] considers the reflectance into the model to make it more appropriate and reasonable for the decomposition, the directly estimated reflectance images shown in Figs. 2(e) and 3(e) appear fuzzy and lose finer details. This is due to the side effect of the logarithmic transformation discussed in Section 2. As can be seen in Figs. 2(f) and 3(f), our reflectance images effectively preserve details and are clearer than that by the Ng's method. Meanwhile, since the illumination is removed, details in dark areas are revealed in the reflectance. Since it is hard to obtain the ground truth of both the reflectance and the illumination, how to quantitatively assess the estimation is a tough problem. In the following content, different experiments are designed to demonstrate the effectiveness of the proposed model and algorithm.

Illumination Adjustment Since the illumination contains the lightness information, removing or adjusting the illumination can generate visually pleasing results for dark images. Therefore, the Gamma correction operation is adopted to modify the estimated illumination. Same as in [11, 26], the Gamma correction of $\mathbf{L}$ with an adjusting parameter γ is defined by:

$$\mathbf{L}' = W\left(\frac{\mathbf{L}}{W}\right)^{\frac{1}{\gamma}}, \tag{9}$$

where W is 255 in an 8-bit image and the empirical parameter γ is set as 2.2. Since the method [11] only estimates the illumination and the method [26] obtains a fuzzy re-

[1]We share our Matlab implementation at: `http://smartdsp.xmu.edu.cn/cvpr2016.html`

(a) input (b) illumination by [11] (c) illumination by [26] (d) our illumination (e) reflectance by [26] (f) our reflectance

Figure 2. Comparison of reflectance and illumination estimation in the RGB domain.

(a) input (b) illumination by [11] (c) illumination by [26] (d) our illumination (e) reflectance by [26] (f) our reflectance

Figure 3. Comparison of reflectance and illumination estimation in the HSV domain. The results look gray because we only show the estimated illumination and reflectance of the V-channel without Hue and Saturation.

flectance, the enhanced images of the two methods is computed by:

$$\mathbf{S}_{enhanced} = (\frac{\mathbf{S}}{\mathbf{L}}) \cdot \mathbf{L}'. \tag{10}$$

While our estimated reflectance preserves finer details, the enhanced image of the proposed method is computed by:

$$\mathbf{S}_{enhanced} = \mathbf{R} \cdot \mathbf{L}'. \tag{11}$$

Fig. 4 shows some examples of illumination adjustment by different methods. A classical image enhancement algorithm based on the center/surround Retinex: multiscale Retinex with color restoration (MSRCR) [9] is also adopted to make a comparison. To preserve color information, the Gamma correction is processed in the HSV domain. As can be seen, MSRCR can effectively enhance details and contrast with color correction. However, this method has over-enhancement to some degree since the estimated illumination is directly removed. The global visual effect of the proposed method is similar to the other two variational methods [11, 26]. This is because adding corrected illumination back to reflectance is a complementary process. However, the proposed method has a better natural performance, such as shadow areas of background in the first row and the clouds in the third row.

Since the ground truth of the enhanced image is unknown, a blind image quality assessment is used to evaluate the enhanced results. This metric is the natural image quality evaluator (NIQE) [22] based on statistical regularities from natural and undistorted images. A lower NIQE value represents a higher image quality and the best results are boldfaced. As shown in Table 1, the proposed method has a lower average than other three methods, in agreement with the our empirical assessment of having the highest quality of enhanced results.

Table 1. Average NIQE values of Fig. 4

	inputs	[9]	[11]	[26]	ours
1st row	2.47	2.35	3.18	2.45	**2.13**
2nd row	2.52	**2.32**	2.70	2.42	2.38
3rd row	3.97	3.54	3.91	**3.46**	3.72
4th row	3.10	2.93	3.62	3.16	**2.77**
Average	3.02	2.79	3.35	2.87	**2.75**

Table 2. Average NIQE values on 300 images

	inputs	[9]	[11]	[26]	ours
Backlit	4.01	3.68	3.43	**3.37**	3.51
Non-uniform	3.47	3.28	3.25	3.33	**3.17**
night-time	5.12	5.01	4.55	4.51	**4.21**

We also test 300 images with different illumination conditions to demonstrate the effectiveness of our model on the Gamma correction. The tested 300 images are selected from the non-uniform illumination image dataset [33], the night-time image dataset [4], the NASA image dataset [25] and the Google image searching. The 300 images are categorized into 16 backlit images, 123 non-uniform illumination images and 164 night-time images. Table 2 shows corresponding average NIQE values of the three categories. As shown in Table 2, the proposed method has the lowest NIQE value on most images, which indicates that our model has a consistent good performance on different kinds of images.

Noise Suppression An important problem of dark image enhancement is how to suppress noise in dark areas when applying the Gamma correction. Two dark images contaminated with slight additive white Gaussian noise **n** with $\sigma = 5$ are processed. Figs. 5 and 6 show the enhanced

(a) inputs (b) results by [9] (c) results by [11] (d) results by [26] (e) our results

Figure 4. Comparison of illumination adjustment.

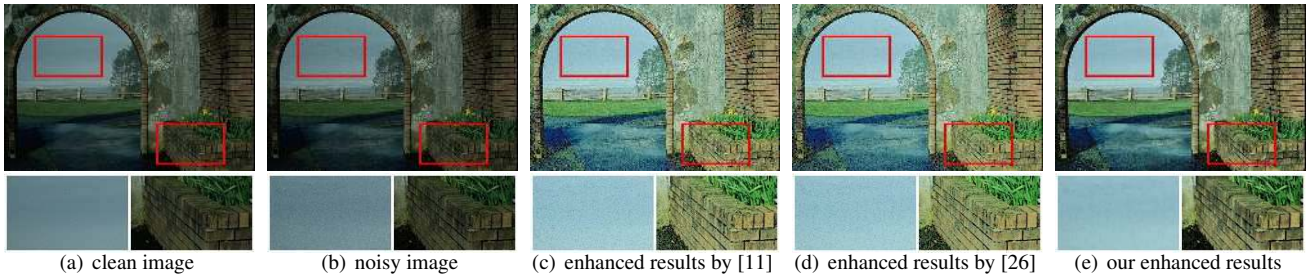

(a) clean image (b) noisy image (c) enhanced results by [11] (d) enhanced results by [26] (e) our enhanced results

Figure 5. Comparison of noise suppression.

(a) clean image (b) noisy image (c) enhanced results by [11] (d) enhanced results by [26] (e) our enhanced results

Figure 6. Comparison of noise suppression.

results with corresponding enlargements in red rectangles. The Gamma correction is processed in the HSV domain. For methods [11, 26], the Gamma correction only relies on the estimated illumination, i.e.,

$$\mathbf{S}_{enhanced} = \frac{\mathbf{S}}{\mathbf{L}} \cdot \mathbf{L}' = (\mathbf{R} \cdot \mathbf{L} + \mathbf{n}) \cdot \frac{\mathbf{L}'}{\mathbf{L}}. \tag{12}$$

It is clear that noise will be amplified after Gamma correction since $\mathbf{L} \leq \mathbf{L}'$ according to Eq. (10). As can be seen in Figs. 5(c) and (d) and Figs. 6(c) and (d), both Kimmel's method [11] and Ng's method [26] amplify the noise after Gamma correction. Since the proposed model estimates reflectance and illumination simultaneously, the L1 regularization term in function (2) can effectively handle noise.

Color Correction As mentioned before, when each RGB channel is estimated separately, the estimated reflectance and illumination contains color information. By removing the illumination, the reflectance retains the original color information of the object, meaning that the proposed model

(a) input (b) ground truth

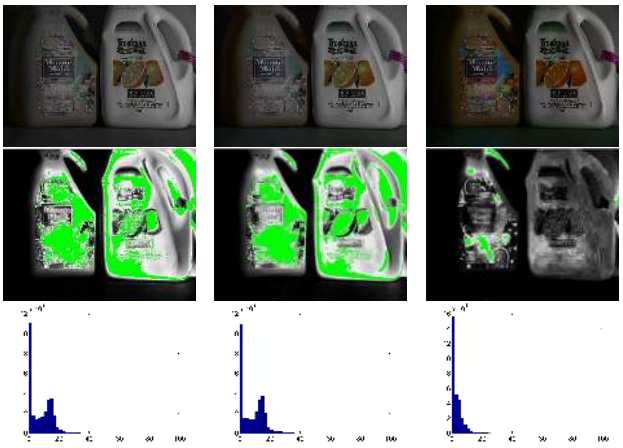

(c) results by [11] (d) results by [26] (e) our results

Figure 7. Comparison of color correction.

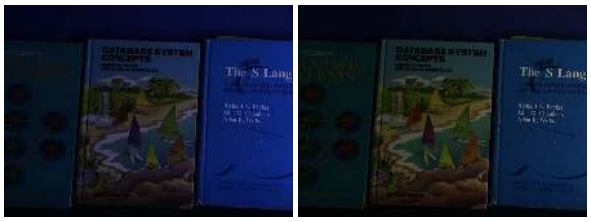

(a) input (b) ground truth

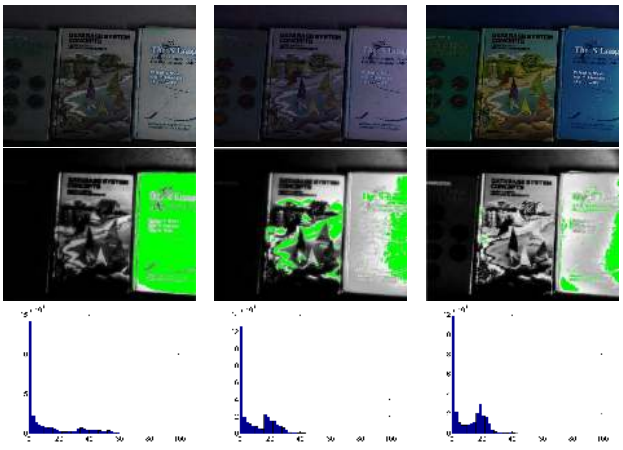

(c) results by [11] (d) results by [26] (e) our results

Figure 8. Comparison of color correction.

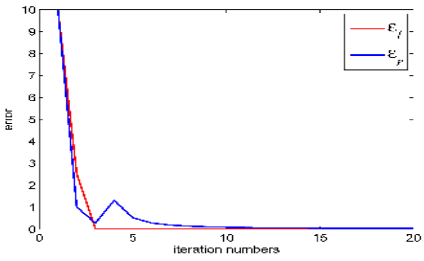

Figure 10. The relation between $\varepsilon_{\mathbf{r}}$, $\varepsilon_{\mathbf{l}}$ and iteration numbers.

has the effect of color correction. In this experiment, the color correction performance is shown in Figs. 7 and 8 to demonstrate the accuracy of the estimated reflectance and illumination. The S-CIELAB color metric [37] based on spatial processing to measure color errors is adopted to verify the accuracy of color correction. The third rows in Figs. 7 and 8 are the corrected results obtained by methods [11, 26] and the proposed one, respectively. The third rows in Figs. 7 and 8 are the spatial location of the errors between the ground truth and other corrected results. The fourth rows in Figs. 7 and 8 are histograms of S-CIELAB errors of the ground truth with other three results, respectively. As can be seen from the spatial locations of the errors, the green areas of our result are smaller than those of other two methods. This indicates that the difference between the ground truth and our result is the smallest, which also can be seen from the histogram distribution of errors. This experiment demonstrates that the proposed model can estimate more accurate results when dealing with color distorted images.

Parameters Impact The impact of regularization parameters c_1 and c_2 on the proposed model (2) is shown in Fig. 9. The default values are set as 0.01 and 0.1. To test the impact of different parameters respectively, we change the value of one parameter while keeping the other one unchanged. As can be seen in Fig. 9, details of estimated reflectance are fuzzed since L1 term decreases as c_1 increases. The estimated illumination smoothed as c_2 increases since c_2 controls the smoothness. In most cases, the empirical setting of regularization parameters generates satisfactory results.

Convergence Rate and Computational Time First, the convergence rate of the proposed algorithm is analyzed. The operation is processed in the HSV domain with a 512×512 image. Fig. 10 shows the relationship between the error $\varepsilon_{\mathbf{r}}$, $\varepsilon_{\mathbf{l}}$ and the number of iterations. As shown from the error curve, the convergence rate is fast. This is due to the approximation strategy and the alternating optimization algorithm are adopted to split the non-convex objective function (2) into three sub-problems that have closed form solutions.

The computational time is also tested since it is an important factor of an algorithm. One hundred images with size of

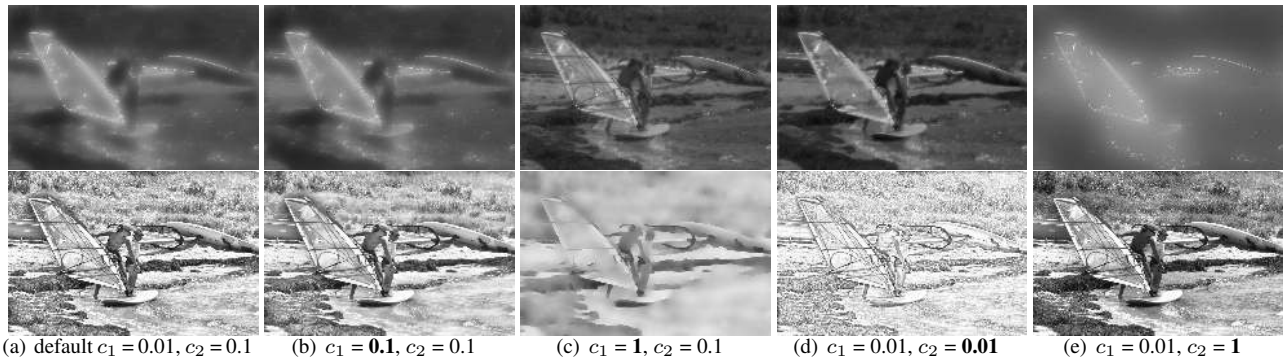

(a) default $c_1 = 0.01$, $c_2 = 0.1$ (b) $c_1 = \mathbf{0.1}$, $c_2 = 0.1$ (c) $c_1 = \mathbf{1}$, $c_2 = 0.1$ (d) $c_1 = 0.01$, $c_2 = \mathbf{0.01}$ (e) $c_1 = 0.01$, $c_2 = \mathbf{1}$

Figure 9. Examples of parameters impact. First row: estimated illumination images. Second row: estimated reflectance images.

Table 3. Average computational times in seconds

	$\varepsilon_1 = \varepsilon_2 = 0.1$	$\varepsilon_1 = \varepsilon_2 = 0.01$	$\varepsilon_1 = \varepsilon_2 = 0.001$
time	0.41	1.79	13.51

512×512 are processed with different stopping parameters ε_1 and ε_2. The operation is processed in the HSV domain and average computational times are shown in Table 3. As can be seen, the smaller stopping parameters is, the higher computational time required. This is due more iterations are required to achieve a smaller error. Note that the experiments are performed by unoptimized Matlab implementation and the computational time can be further improved by C programming and advanced computing devices.

Extension: Illumination Invariant Facial Images Finally, the proposed model is used to process illumination invariant facial images. In this experiment, the reflectance is estimated by the new model over four images [15, 36] under different illumination conditions. As can be seen in Fig. 11, though the person's face is affected by different lighting conditions, the estimated reflectance is similar since the illumination is well estimated and eliminated from the observed images. This experiment shows that the proposed model has the potential to be used in other computer vision applications.

(a) observed facial images

(b) corresponding reflectance images

Figure 11. Processing illumination invariant facial images.

5. Conclusion

In this paper, a new weighted variational model for simultaneous estimation of reflectance and illumination is introduced. First, we show the side effect of the logarithmic transformation. Based on the analysis of the logarithmic transformation, a weighted variational model is introduced to refine the regularization terms for better prior representation. An alternating minimization algorithm with an approximation strategy is adopted to estimate the model. We present a comprehensive experimental analysis of the proposed model using both subjective and objective assessments. Compared with other testing methods, the proposed one shows similar or even better results with satisfactory convergence rate and computational times.

6. Acknowledgements

We would like to thank the anonymous reviewers for their helpful feedback. This work was supported in part by the National Natural Science Foundation of China under Grants 61571382, 61571005, 81301278, 61172179 and 61103121, in part by the Guangdong Natural Science Foundation under Grant 2015A030313007, in part by the Fundamental Research Funds for the Central Universities under Grants 20720160075, 20720150169 and 20720150093, and in part by the Research Fund for the Doctoral Program of Higher Education under Grant 20120121120043.

References

[1] M. Bertalmío, V. Caselles, , E. Provenzi, and A. Rizzi. Perceptual color correction through variational techniques. *IEEE Trans. Image Process.*, 16(4):1058–1072, 2007.

[2] M. Bertalmío, V. Caselles, and E. Provenzi. Issues about Retinex theory and contrast enhancement. *Int. J. Comput. Vision*, 83(1):101–119, 2009.

[3] H. Chang, M. K. Ng, W. Wang, and T. Zeng. Retinex image enhancement via a learned dictionary. *Optical Engineering*, 54(1):013107–1–013107–15, 2015.

[4] Z. Chen, T. Jiang, and Y. Tian. Quality assessment for comparing image enhancement algorithms. In *IEEE Conference on Computer Vision and Pattern Recognition (CVPR)*, pages 3003–3010, Ohio, June 2014.

[5] B. Funt, F. Ciurea, and J. McCann. Retinex in matlab. *J. Electron. Imaging*, 13(1):48–57, 2004.

[6] T. Goldstein and S. Osher. The split Bregman method for L1-regularized problems. *SIAM J. Imaging Sci.*, 2(2):323–343, 2009.

[7] B. Gu, W. Li, M. Zhu, and M. Wang. Local edge-preserving multiscale decomposition for high dynamic range image tone mapping. *IEEE Trans. Image Process.*, 22(1):70–79, 2013.

[8] B. K. P. Horn. Determining lightness from an image. *Comput. Graphics Image Process.*, 3(4):277–299, 1974.

[9] D. J. Jobson, Z. U. Rahman, and G. A. Woodell. A multiscale Retinex for bridging the gap between color images and the human observation of scenes. *IEEE Trans. Image Process.*, 6(7):965–976, 1997.

[10] C. Jung, T. Sun, and L. Jiao. Eye detection under varying illumination using the Retinex theory. *Neurocomput.*, 113:130–137, 2013.

[11] R. Kimmel, M. Elad, D. Shaked, R. Keshet, and I. Sobel. A variational framework for Retinex. *Int. J. Comput. Vision*, 52(1):7–23, 2003.

[12] X. Lan, H. Shen, L. Zhang, and Q. Yuan. A spatially adaptive Retinex variational model for the uneven intensity correction of remote sensing images. *Signal Process.*, 101:19–34, 2014.

[13] E. H. Land. *The Retinex theory of color vision*. Sci. Amer., 1977.

[14] E. H. Land and J. J. McCann. Lightness and Retinex theory. *J. Opt. Soc. Am.*, 61(1):1–11, 1971.

[15] K. C. Lee, J. Ho, and D. J. Kriegman. Acquiring linear subspaces for face recognition under variable lighting. *IEEE Trans. Pattern Anal. Mach. Intell.*, 27(5):684–698, 2005.

[16] H. Li, L. Zhang, and H. Shen. A perceptually inspired variational method for the uneven intensity correction of remote sensing images. *IEEE Trans. Geosci. Remote Sens.*, 50(8):3053–3065, 2012.

[17] J. Liang and X. Zhang. Retinex by higher order total variation decomposition. *J. Math. Imaging Vis.*, 52(3):345–355, 2015.

[18] Y. Liu, R. R. Martin, L. D. Domincis, and B. Li. Using Retinex for point selection in 3D shape registration. *Pattern Recogn.*, 47(6):2126–2142, 2014.

[19] W. Ma, J. M. Morel, S. Osher, and A. Chien. An L1-based variational model for Retinex theory and its applications to medical images. In *IEEE Conference on Computer Vision and Pattern Recognition (CVPR)*, pages 153–160, 2011.

[20] W. Ma and S. Osher. A TV bregman iterative model of Retinex theory. *Inverse Problems and Imaging*, 6(4):697–708, 2012.

[21] J. McCann. Lessons learned from mondrians applied to real images and color gamuts. In *Proc. IS&T/SID 7th Color Imag. Conf.*, pages 1–8, 1999.

[22] A. Mittal, R. Soundararajan, and A. C. Bovik. Making a completely blind image quality analyzer. *IEEE Signal Process. Lett.*, 20(3):209–212, 2013.

[23] J. M. Morel, A. B. Petro, and C. Sbert. A PDE formalization of Retinex theory. *IEEE Trans. Image Process.*, 19(11):2825–2837, 2010.

[24] Y. Nam, D. Choi, and B. Song. Power-constrained contrast enhancement algorithm using multi-scale Retinex for oled display. *IEEE Trans. Image Process.*, 23(8):3308–3320, 2014.

[25] NASA. Retinex image processing. 2001. `http://dragon.larc.nasa.gov/retinex/pao/news/`.

[26] M. K. Ng and W. Wang. A total variation model for Retinex. *SIAM J. Imaging Sci.*, 4(1):345–365, 2011.

[27] S. Osher, M. Burger, D. Goldfarb, J. Xu, and W. Yin. An iterative regularization method for total variation-based image restoration. *Multiscale Model. Simul.*, 4(2):460–489, 2005.

[28] R. Palma-Amestoy, E. Provenzi, M. Bertalmío, and V. Caselles. A perceptually inspired variational framework for color enhancement. *IEEE Trans. Pattern Anal. Mach. Intell.*, 31(3):458–474, 2009.

[29] S. Pan, X. An, and H. He. Adapting iterative Retinex computation for high-dynamic-range tone mapping. *J. Electron. Imaging*, 22(2):023006–1–023006–10, 2013.

[30] E. Provenzi, L. D. Carli, A. Rizzi, and D. Marini. Mathematical definition and analysis of the Retinex algorithm. *J. Opt. Soc. Amer. A*, 22(12):2613–2621, 2005.

[31] W. F. Schreiber. *Fundamentals of electronic imaging systems*. Springer, 1986.

[32] L. Wang, L. Xiao, H. Liu, and Z. Wei. Variational Bayesian method for Retinex. *IEEE Trans. Image Process.*, 23(8):3381–3396, 2014.

[33] S. Wang, J. Zheng, H. M. Hu, and B. Li. Naturalness preserved enhancement algorithm for non-uniform illumination images. *IEEE Trans. Image Process.*, 22(9):3538–3548, 2013.

[34] W. Wang and C. He. A variational model with barrier functionals for Retinex. *SIAM J. Imaging Sci.*, 8(3):1955–1980, 2015.

[35] W. Wang and M. K. Ng. A nonlocal total variation model for image decomposition: illumination and reflectance. *Numerical Mathematics: Theory, Methods and Applications*, 7(3):334–355, 2014.

[36] Yale. The extended Yale face database B. 2001. `http://vision.ucsd.edu/~iskwak/ExtYaleDatabase/ExtYaleB.html`.

[37] X. Zhang and B. A. Wandell. A spatial extension of CIELAB for digital color image reproduction. In *SID international symposium digest of technical papers*, volume 27, pages 731–734, 1996.

[38] Q. Zhao, P. Tan, Q. Dai, L. Shen, E. Wu, and S. Lin. A closed-form solution to retinex with nonlocal texture constraints. *IEEE Trans. Pattern Anal. Mach. Intell.*, 34(7):1437–1444, 2012.

[39] D. Zosso, G. Tran, and S. J. Osher. Non-local Retinex—a unifying framework and beyond. *SIAM J. Imaging Sci.*, 8(2):787–826, 2015.